Quantum chemical sensing using molecular triplet qubits in a flexible metal–organic framework

Akio Yamauchi,[1] Saiya Fujiwara,[3] Nobuo Kimizuka,[1,2] Mizue Asada,[4] Motoyasu Fujiwara,[4] Toshikazu Nakamura,[4] and Nobuhiro Yanai.*[1,2,5]

[1] Department of Applied Chemistry, Graduate School of Engineering and [2] Center for Molecular Systems (CMS), Kyushu University, 744 Moto-oka, Nishi-ku, Fukuoka 819-0395, Japan.

[3] RIKEN, RIKEN Center for Emergent Matter Science, Wako, Saitama 351-0198, Japan.

[4] Institute for Molecular Science, Nishigonaka 38, Myodaiji, Okazaki 444-8585, Japan .

[5] FOREST, JST, Honcho 4-1-8, Kawaguchi, Saitama 332-0012, Japan.

*Corresponding author. E-mail: yanai@mail.cstm.kyushu-u.ac.jp

Abstract:
Quantum sensing using molecular qubits is expected to provide excellent sensitivity due to the proximity of the sensor to the target analyte. However, many molecular qubits are used at cryogenic temperatures, and how to make molecular qubits respond to specific analytes remains unclear. Here, we propose a new quantum sensor design in which the coherence time changes in response to a variety of analytes at room temperature. We used the photoexcited triplet, which can be initialized at room temperature, as qubits and introduce them to a metal–organic framework that can flexibly change its pore structure in response to guest adsorption. By changing the local molecular density around the triplet qubits by adsorption of a specific analyte, the mobility of the triplet qubit can be changed, and the coherence time can be made responsive.

Introduction

In the second quantum revolution, quantum information science (QIS) comprises the application of quantum mechanics to fields such as quantum computing[1,2], quantum communication[3,4], and quantum sensing[5-10]. Quantum bits (qubits) are its building blocks, and manipulating these superposition states creates new properties that cannot be achieved by classical bits[11,12]. Among the quantum technologies, quantum sensing will have an impact on a wide range of fields, including chemistry[9] and biology[10]. Quantum sensing is defined as satisfying one or, in a narrower sense, all of the following three conditions[5]: (i) the use of qubits (two levels), qutrits (three levels), or qunuts (*n* levels) to measure physical quantities; (ii) the use of quantum coherence to measure physical quantities; and (iii) the use of quantum entanglement to improve the sensitivity and accuracy of measurements. An important parameter for quantum sensing is the time over which the coherence of spin correlations is preserved[13]. Since the sensitivity of quantum sensing depends on coherence time, a long coherence time is highly desirable[5]. Defect centers, such as the nitrogen-vacancy (NV) centers in diamond, have long coherence times of more than microseconds at room temperature, enabling sensing of a variety of small molecules and biomolecules[8,10]. However, defect centers are difficult to place in a specific position, and it is also difficult to selectively address different centers[14].

Unlike defect-based systems, molecular qubits[14-31] are uniform in structure and can be precisely controlled. Furthermore, their small size allows them to closely approach the target analyte. For electron spin-based systems, the coherence time can be determined as the spin–spin relaxation time (T_2). Paramagnetic metal complexes[15-18], radical pairs[22], and metal complex-radical conjugates[24-26] are typical examples of molecular qubits. Recent research efforts have realized high T_2 values at low temperature by appropriate molecular design, but it remains challenging to achieve microsecond-scale T_2 at room temperature. Furthermore, it remains unclear how to make molecular qubits responsive and selective to specific analytes.

Except for a few pioneering examples[27-30], photoexcited triplets are largely unexplored in the context of qubits. Photoexcited triplet states have the advantage that anisotropic spin-orbit coupling (SOC) allows temperature-independent sublevel selective intersystem crossing (ISC) from the photoexcited singlet state, creating highly polarized electronic states, even at room temperature[32-35] (Fig. 1a). This is a major difference from the spins of metal complexes and radicals in thermal equilibrium, and

triplets can offer higher spin polarization than those systems at room temperature and low magnetic fields. Furthermore, it has long been known that the triplet state of pentacene doped in dense *p*-terphenyl crystals exhibits a long T_2 on the microsecond scale even at room temperature[33]. However, triplets have never been used for quantum sensing because they are buried in dense matrix crystals and cannot approach the target analyte.

Here, we propose a new quantum sensing strategy in which triplet qubits are supported in nanoporous metal–organic frameworks (MOFs) to make the analyte molecules accessible, and the coherence time T_2 of the triplet qubits is changed by flexibly changing the MOF structure through adsorption of the guest analyte. Although a few examples of quantum sensing using MOFs containing paramagnetic species in thermal equilibrium have been reported[36,37], there have been no examples of using the non-equilibrium highly-polarized state, such as triplets, at room temperature, or using the flexible structure of MOFs to obtain different responses for the type of guest analyte.

We selected MIL-53 as a flexible MOF that exhibits guest-responsive structural change, termed 'breathing' behavior[38-40]. One of the unique features of MOFs is that the crystal structure can be flexibly changed by adsorption and desorption of guest molecules[41-43]. The N-substituted tetracene, 5,12-diazatetracene (DAT)[32], was employed as the triplet qubit. Compared with conventional pentacene, DAT has the advantages of good solubility and superior air-stability. Recently, we reported the successful introduction of DAT into MIL-53 nanopores and polarization transfer from the electron spins of the DAT triplet to the ^{19}F nuclear spins of the guest fluorouracil[44].

In this work, we introduced a variety of guest molecules into DAT-accommodated MIL-53 and evaluated T_2 of the DAT triplet using pulsed electron paramagnetic resonance (EPR) (Fig. 1b). Analyte molecules have nuclear spins, such as that on protons, which usually work as noise to shorten T_2. Interestingly, the T_2 of DAT in MIL-53 shows various T_2 depending on the type of guest analyte, with the longest T_2 being longer than 1 μs at room temperature. This can be attributed to the local molecular density around the DAT and has led to a new concept of quantum sensing by controlling the dynamics of qubits.

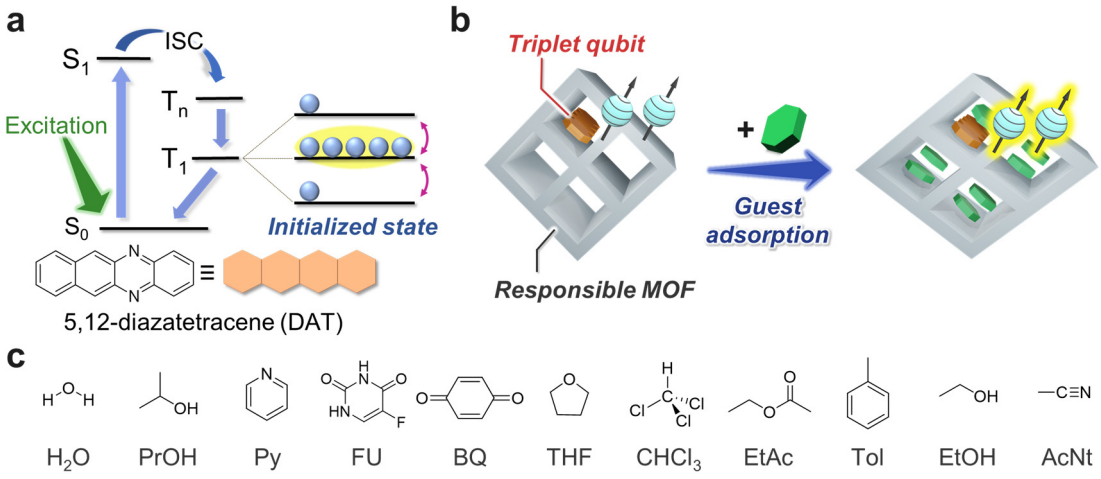

Fig. 1. Quantum sensing using triplet qubits and a flexible MOF. a, Initialization of the triplet qubit. Two of the three triplet sublevels generated by photoexcitation can be

used as qubits. **b**, Response of triplet qubits to the guest-induced structural change of a flexible MOF. DAT and D-MIL-53 are employed as triplet qubits and the flexible MOF, respectively. **c**, Guest molecules used in this research.

Results and discussion

DAT was introduced into partially deuterated MIL-53 [Al(μ_2-OH)(BDC-d_4)]$_n$ (denoted as D-MIL-53⊃DAT; BDC-d_4 = perdeuterated terephthalate) by simply soaking D-MIL-53 in a DAT solution, according to our previous report[44]. The loading amount of DAT was estimated to be 0.87 wt% by UV–Vis absorbance after digesting D-MIL-53 (Fig. S1), similar to our previous report[44]. The following 11 guests were introduced into D-MIL-53⊃DAT: H_2O, 2-propanol (PrOH), pyridine (Py), 5-fluorouracil (FU), *p*-benzoquinone (BQ), THF, chloroform ($CHCl_3$), ethyl acetate (EtAc), toluene (*h*-Tol), ethanol (EtOH), and acetonitrile (AcNt). FU and BQ were introduced by sublimation, and other guests were introduced by exposing D-MIL-53 to each vapor.

Guest-dependent coherence time (T_2). The coherence times (T_2) of the photoexcited triplets of DAT in D-MIL-53 were measured by pulsed EPR at room temperature with a spin echo sequence varying the pulse intervals (Fig. 2a). Measurements were taken at the magnetic field of the high-field and low-field peaks of the EPR spectra shown later, respectively, and both decay curves are shown (Fig. 2c). The decay of echo intensity was fitted with a single exponential function and T_2 was obtained as the decay constant. While DAT shows electron spin echo envelope modulation (ESEEM) due to hyperfine coupling with ^{1}H nuclei and ^{14}N nuclei at higher magnetic field, it does not affect the estimation of T_2. The T_2 values obtained at the higher and lower magnetic fields are similar (Table S1). A relatively short T_2 of around 0.1 μs is observed for D-MIL-53⊃DAT without any guest analyte (termed 'empty'). No echo signals are detected when *h*-Tol, EtOH, or AcNt are introduced as guests, probably due to the shortening of T_2 (< 0.1 μs). This is not surprising, since proton nuclear spins usually work as noise and reduce coherence time[13]. Meanwhile, interestingly, the introduction of some guest molecules such as Py, FU, BQ, and THF clearly elongate T_2 of the DAT triplets, despite the increase in proton and other nuclear spins that could cause spin relaxation. The T_2 of DAT in the presence of FU and BQ are over 1 μs, which are notably long values as molecular qubits at room temperature.

The T_2 value was plotted against the cell volume of MIL-53 (Fig. 2b). With increasing cell volume, T_2 shows a non-monotonic trend, becoming longer and then shorter. Triplet qubit and flexible MOF hybrids exhibit different coherence times for various guest molecules, enabling room-temperature quantum chemical sensing of neutral molecules that has not been reported previously.

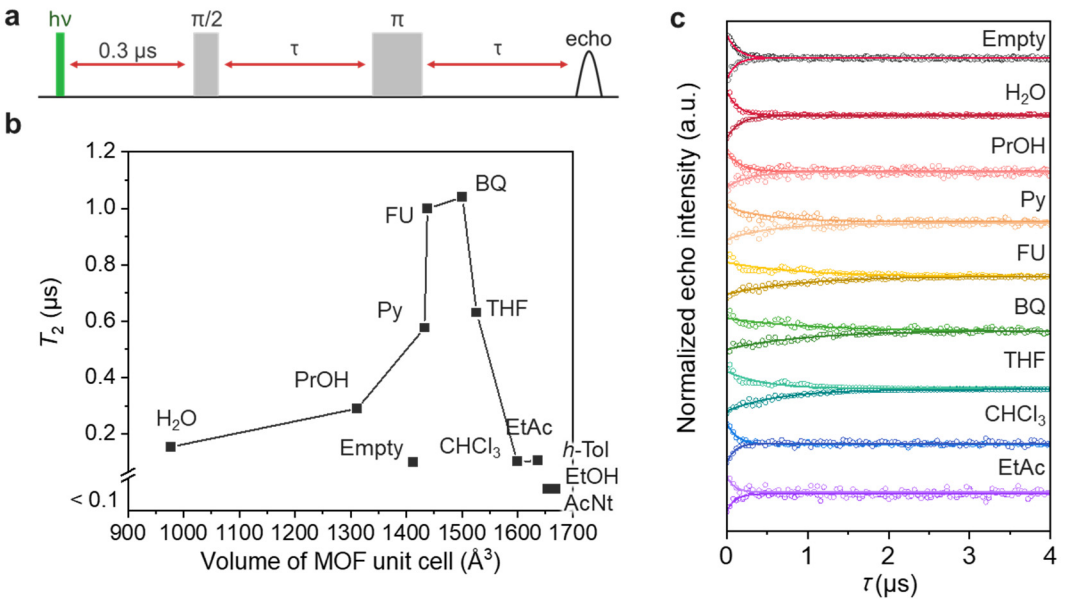

Fig. 2. Guest-dependent T_2 of DAT triplets in D-MIL-53. a, Spin echo sequence used for T_2 measurement. The intervals of microwave pulses and echo detection were varied. **b**, Plot of T_2 obtained by the single-exponential fitting of the spin echo decay curves against the unit cell volume of MIL-53. Only the T_2 obtained from the low field peaks where the effect of ESEEM was small is plotted. **c**, Spin echo decay curves after pulsed photoexcitation at 532 nm for empty (D-MIL-53⊃DAT) and guest-filled (D-MIL-53⊃[DAT+guest]) samples at room temperature. The decay curves of each sample at the magnetic field corresponding to the higher and lower EPR peaks (Fig. 3a) are shown at the top and bottom, respectively. Single-exponential fitting curves for each sample are also shown. Echo signals were not observed when the guest was *h*-Tol, EtOH, or AcNt.

Possible mechanism of guest-dependent T_2. To obtain information about the interaction of DAT with guest molecules in the ground and excited triplet state, we obtained UV–Vis absorption and time-resolved EPR spectra, respectively. For D-MIL-53⊃[DAT+H_2O] (MIL-53 immediately absorbs water and forms a hydrated structure), DAT shows absorption peaks at 450, 480, and 515 nm derived from π–π* transitions. This is consistent with the absorption peaks of DAT molecularly dispersed in *p*-terphenyl and is clearly different from the red-shifted peaks of DAT in its aggregated solid state, as we previously reported[32] (Fig. S2). With the exception of BQ, where the guest itself shows absorption, no significant change in the absorption spectrum is observed when various guest molecules are introduced (Fig. S3). This indicates that the interaction between DAT and the guest molecules is small in the ground state and that DAT is not aggregated by the introduction of guests.

Figure 3a shows the time-resolved EPR spectra of the DAT triplet in D-MIL-53 in the absence and presence of guest molecules. All the samples show similar EPR spectra typical for a polarized DAT triplet. The EPR spectra were simulated using the EasySpin toolbox[45] in MATLAB (red lines in Fig. 3a, Table S1). There are no large differences in the relative zero-field populations (P_x : P_y : P_z) and zero-field splitting parameters (*D*

and *E*) between the samples, indicating the absence of strong electronic interactions between the DAT triplet and guest analytes.

The spin–lattice relaxation time (T_1) was estimated from the decay of the EPR signal after light irradiation (Fig. 3b). The T_1 value for each sample is more than an order of magnitude longer than the corresponding T_2 value, indicating that T_2 is not dominated by T_1 (Fig. S4, Table S1). The guest-dependence of T_1 shows a similar trend to that of T_2, with some exceptions (such as water). This result suggests that additional relaxation mechanisms exist for spin–spin relaxation.

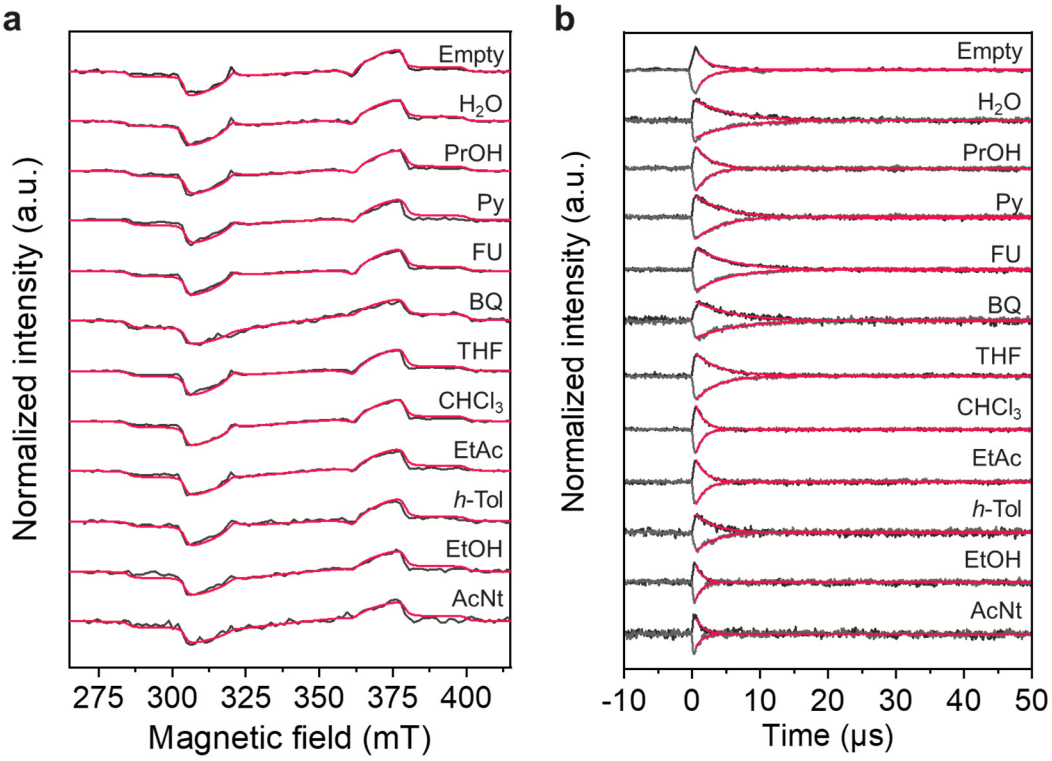

Fig. 3. Time-resolved EPR measurements of DAT in D-MIL-53. a, Time-resolved EPR spectra at 0.1–0.5 μs for empty (D-MIL-53⊃DAT) and guest-filled (D-MIL-53⊃[DAT+guest]) samples at room temperature. The simulated EPR spectra are shown as red lines. **b**, Decays of the ESR peaks at higher and lower magnetic field after pulsed photoexcitation at 532 nm for empty (D-MIL-53⊃DAT) and guest-filled (D-MIL-53⊃[DAT+guest]) samples at room temperature. Decay curves were fitted by a single exponential function and the fitting results are shown as red curves.

To gain insight into the local molecular density around DAT in the MOF nanopores, thermogravimetric analysis (TGA) was performed (Fig. S5). The MOF cell volume minus the framework volume was approximated as the pore volume, and the volume fraction of the pore volume occupied by the guest was estimated. Interestingly, the larger the volume fraction occupied by the guest, the longer the T_2 (Fig. 4). *h*-Tol does not fit this trend, and it is possible that the rotation of the methyl group is responsible for shortening T_2[13]. When perdeuterated toluene (*d*-Tol) is introduced as a guest, T_2 for

the DAT triplet id extended to ~0.3 μs (Fig. S6), which matches the trend for the other guest molecules. This suggests that, in the absence of a particularly relaxing substituent such as a methyl group, the higher the volume fraction occupied by guest (or local molecular density), the more the motility of DAT is suppressed and the longer T_2 is. As for the terephthalate ligand of MIL-53, there is no change in T_2 for the DAT triplet in the deuterated and protonated forms. There is little change in the T_2 of the DAT triplet when H_2O and D_2O are used as guest molecules.

These results suggest that the spin–spin relaxation is mainly affected by the motion of DAT itself rather than the surrounding nuclear spins. Further analysis using techniques such as solid-state NMR and terahertz spectroscopy may reveal the detailed dynamics of DAT, but the amount of DAT incorporated into MOF is only 0.87 wt%, so is difficult to get such insights due to the much larger amounts of host ligands and other guest molecules present.

To support the idea that DAT dynamics is the main factor determining T_2, we measured T_2 at lower temperatures in the empty, guest-free state (D-MIL-53⊃DAT) (Fig. S7). The T_2 of the DAT triplet, which is 0.1 μs at room temperature, is longer at 100 and 50 K at 1.0 and 2.8 μs, respectively. Conversely, in *p*-terphenyl, which is a solid and dense crystal, the DAT triplet shows a long T_2 of 2.4 μs, even at room temperature. These results indicate that magnetic field fluctuations based on the molecular motion of DAT, such as librational motion, are the main cause of spin–spin relaxation[13].

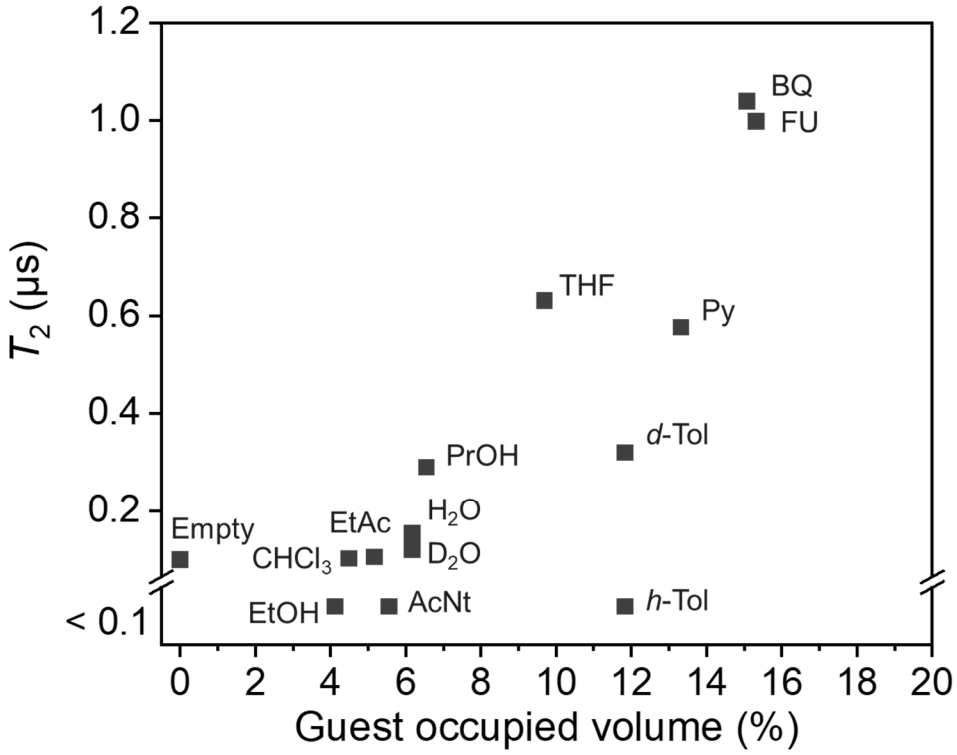

Fig. 4. Dependence of T_2 on volume fraction occupied by the guest. T_2 and volume fraction occupied by the guest are plotted for empty (D-MIL-53⊃DAT) and guest-filled (D-MIL-53⊃[DAT+guest]) samples.

Conclusions

This study is the first to demonstrate quantum sensing of diverse neutral molecules by hybridizing triplet qubits in flexible MOFs. The photoexcited triplet, which is initializable at room temperature and exhibits a long coherence time (T_2), was used as qubits, and the MOF, which can flexibly change its structure upon adsorption of various analyte molecules, was used to make the qubits responsive. Since there are many examples of MOFs selectively adsorbing specific guests or showing abrupt adsorption at a certain pressure, numerous quantum sensors that read the type and concentration of molecules could be realized. Furthermore, by introducing various triplet qubits into flexible and rigid MOFs as guest molecules or ligands, a "quantum nose" that can distinguish a wide range of molecule types could be realized. The control of MOF orientation is expected to enable more advanced quantum sensing by sophisticated qubit manipulation. Triplets can also be detected optically by phosphorescence and delayed fluorescence, leading to highly sensitive sensing and, ultimately, to single molecule quantum sensing[27,46]. The triplet-MOF complex will provide an ultra-sensitive and highly selective quantum sensing platform that will have impact in a wide range of fields such as analytical chemistry, life sciences, and medicine.

Methods

All reagents were used as received unless otherwise noted. Aluminum chloride hexahydrate ($AlCl_3 \cdot 6H_2O$) and *p*-benzoquinone (BQ) were purchased from Sigma-Aldrich. *p*-Terphenyl was purchased from FUJIFILM Wako Pure Chemical and purified by zone melting. *o*-Phenylenediamine, potassium dichromate ($K_2Cr_2O_7$), and ethylenediamine-*N,N,N′,N′*-tetraacetic acid, tetrasodium salt tetrahydrate (Na_4-EDTA) were purchased from FUJIFILM Wako Pure Chemical. 2,3-Dihydroxynaphthalene and 5-fluorouracil (FU) were purchased from TCI. Glacial acetic acid and oxalic acid dihydrate were purchased from Kishida Chemical. Terephthalic acid-d_4 (BDC-d_4) (ring-d_4, 98 atom%) was purchased from Cambridge Isotope Laboratories, Inc. 5,12-Diazatetracene (DAT) and deuterated MIL-53 (D-MIL-53) were prepared following the literature with slight modifications[32,47].

General characterization

Solution-state ^{1}H-NMR (400 MHz) spectra were recorded on a JEOL JNM-ECZ400 spectrometer using TMS as the internal standard. Elemental analysis was carried out using a Yanaco CHN Corder MT-5 at the Elemental Analysis Center, Kyushu University. UV–Vis absorption spectra were obtained on a JASCO V-670 spectrophotometer. Fluorescence spectra were obtained using a JASCO FP-8700 fluorescence spectrometer. Thermogravimetric analysis curves were obtained on a Rigaku Thermo Plus EVO2 under N_2.

Sample preparation

The samples were prepared according to a previously reported method with slight modifications[32,47].

Synthesis of DAT

A mixture of 2,3-dihydroxynaphthalene (2.00 g, 12.5 mmol) and *o*-phenylenediamine (1.35 g, 12.5 mmol) was put into a 50 mL flask and heated to 200 ℃ for 1 h under N_2 atmosphere. After

filtering and washing the crude product with methanol, 5,12-dihydrodibenzo[b]phenazine was obtained as a yellow solid and used in the next step without further purification.

5,12-Dihydrodibenzo[b]phenazine (2.04 g, 8.69 mmol) was added to 60 mL of glacial acetic acid to produce a suspension. $K_2Cr_2O_7$ (5.32 g, 18.0 mmol) in 20 mL water was slowly added dropwise, and the mixture was stirred overnight in the dark at room temperature. After neutralization, the organic layer was extracted with $CHCl_3$, dried with anhydrous Na_2SO_4, and concentrated under reduced pressure. Recrystallization from toluene gave 5,12-diazatetracene (DAT) as a reddish-orange solid (yield: 47%).

^{1}H-NMR (400 MHz, $CDCl_3$, TMS): δ (ppm) = 8.92 (s, 2H), 8.23 (dd, 2H), 8.13 (dd, 2H), 7.81 (dd, 2H), 7.54 (dd, 2H).

Elemental analysis for $C_{16}H_{10}N_2$: calculated (%) H 4.38, C 83.46, N 12.17; found (%) H 4.30, C 83.50, N 12.03.

Synthesis of D-MIL-53

$AlCl_3 \cdot 6H_2O$ (966 mg, 4 mmol), oxalic acid dihydrate (504 mg, 4 mmol), and terephthalic acid-d_4 (BDC-d_4) were added to 30 mL deionized H_2O and put into a 50 mL Teflon-lined autoclave. The mixture was sonicated, heated at 220 ℃ for 72 h, and cooled to room temperature over 24 h in an oven. After filtering and washing the product with DMF and methanol, a colorless powder was obtained.

To remove the residual BDC-d_4 ligands from D-MIL-53, the obtained powder was added to 15 mL DMF and heated to 120 ℃ for 16 h in the oven again. The resulting product was filtered and washed with DMF and methanol. These procedures were repeated until the peak from BDC-d_4 was no longer observed in thermogravimetric measurements (at least three times). The product was then activated at 150 °C for 3 h.

In ambient air, activated MIL-53 immediately adsorbs water molecules and forms hydrated structures[39] (denoted as D-MIL-53⊃water).

Elemental analysis for $[C_8H_{1.08}D_{3.92}O_5Al_1] \cdot 1.0(H_2O)$: calculated (%) H 3.06, C 41.75, N 0.00; found (%) H 3.05, C 41.80, N 0.00.

Introduction of DAT into D-MIL-53

D-MIL-53 (50 mg) was put into a 6 mL vial and dried under reduced pressure at room temperature over 3 h. The vial was placed in the dark for 1 h at room temperature after adding 2.5 mL dichloromethane solution of DAT (1 mM). The mixture was centrifuged, washed with fresh dichloromethane (1.0 mL, seven times), and dried under vacuum at 100 °C for 3 h. D-MIL-53⊃DAT was obtained as a yellow powder.

In the ambient air, D-MIL-53⊃DAT quickly absorbs water and forms the hydrated structure (denoted as D-MIL-53⊃[DAT+water]).

Quantification of the number of DAT molecules in D-MIL-53⊃DAT

The amount of DAT molecules in D-MIL-53 was calculated by UV–Vis absorbance after digesting D-MIL-53⊃DAT in aqueous Na_4-EDTA solution. DAT was extracted from 20.0 mg D-MIL-53⊃DAT using 4.0 mL dichloromethane after adding 4.0 mL aqueous Na_4-EDTA solution (125 mM). The absorbance at 475 nm of the dichloromethane solution of DAT was 0.055 in a 1 mm cell for 20.0 mg of D-MIL-53⊃[DAT+water]. From the calibration curve, the concentration of the solution was calculated to be 0.175 mM. Therefore, the total amount of DAT in the 4.0 mL dichloromethane solution was found to be 0.70 μmol (= 0.16 mg). Since 7.8 wt% of water was contained in D-MIL-53⊃[DAT+water] (from the TGA curve), the weight of D-MIL-53⊃DAT without water was determined to be 18.44 mg (86.95 μmol). Thus, the number of DAT molecules per unit cell of D-MIL-53 was estimated to be 0.70/86.95 = 0.008, which corresponds to 0.87 wt% of DAT in D-MIL-53⊃DAT.

Introduction of guests into D-MIL-53⊃DAT

Guest analytes (except for 5-fluorouracil (FU) and *p*-benzoquinone (BQ)) were introduced by exposing D-MIL-53⊃DAT to each guest vapor. D-MIL-53⊃DAT was put into a 6 mL vial and dried under reduced pressure at 80 °C for 3 h. The vial was placed in a Schlenk flask containing

a small amount of solvent containing activated 3A molecular sieves and stored in the dark overnight.

The introduction of FU and BQ into the nanochannels of D-MIL-53⊃DAT was performed by the sublimation method[48]. D-MIL-53⊃DAT was evacuated at room temperature for 3 h. FU (35 mg) or BQ (60 mg) were added to D-MIL-53⊃DAT and the mixtures were put into a 30 mL Schlenk flask. After 1 h of evacuation, guests were sublimated and absorbed directly into the nanopores of the MOF at 175 °C for FU and 80 °C for BQ under reduced pressure for 1 h. Residual guests were eliminated at 175 °C or 80 °C under vacuum until the PXRD peaks of bulk FU and BQ were no longer observed. D-MIL-53⊃[DAT+FU] and D-MIL-53⊃[DAT+BQ] were obtained as a pale-yellow powder and a yellow powder, respectively.

Sample preparation for EPR measurements

Samples used in the EPR measurements were prepared as follows: D-MIL-53⊃[DAT+guests] were put into 2 mm capillaries, which were plugged with cotton wool to avoid sample scattering. For liquid guests, a small amount of guest was added to the cotton wool to maintain the vapor pressure. The capillaries were degassed under 77 K for more than 30 min with an oil pump and sealed with a flame.

EPR spectroscopy

EPR measurements were performed on a Bruker E680 operated at X-band (~9.6 GHz) using 2 mm glass capillaries placed into 4 mm quartz EPR tubes. The samples were excited at a wavelength of 532 nm, excitation light intensity of 2~3 mJ/pulse, and repetition rate of 30 Hz using a Spectra-Physics Quanta-Ray YAG laser. The microwave intensities were ~0.06 mW for time-resolved measurements and ~2 μW for pulsed EPR measurements. Temperature was controlled by flowing liquid helium using an Oxford Mercury iTC. The echo decay measurements were conducted using a two-pulse spin echo sequence. The first π/2 pulse was irradiated 0.3 μs after laser excitation and the pulse interval τ was varied. T_2 was obtained by single exponential fitting of decay curves.

Estimation of guest density

The number of guest molecules per unit cell of D-MIL-53 (n_{guest}) was calculated from the following equation (Table S2):

$$n_{guest} = \frac{w_{loss}(m_{MOF} + n_{DAT}m_{DAT})}{m_{guest}(1 - w_{loss})}$$

where w_{loss}, n_{DAT}, m_{MOF}, m_{DAT} and m_{guest} are weight loss (weight of guest) as a percentage of total weight, the number of DAT molecules per unit cell of D-MIL-53, the molecular weight of D-MIL-53, the molecular weight of DAT, and the molecular weight of the guest, respectively. The pore volume per MOF unit cell (V_{pore}) of MIL-53⊃water was obtained as 638 Å^3 by Platon software. By subtracting this V_{pore} from the volume of the MOF unit cell of MIL-53⊃H_2O (V_{MOF}, 977 Å^3)[39], the volume of the framework ($V_{structure}$) was estimated as 339 Å^3. This $V_{structure}$ was assumed to be same for all the D-MIL-53⊃[DAT+guest]. The percentage of guest occupied volume was estimated by the following equation,

$$guest\ \ occupied\ \ volume\ \ (\%) = \frac{100 n_{guest} V_{guest}}{V_{MOF} - V_{structure}} = \frac{100 n_{guest} V_{guest}}{V_{pore}}$$

where V_{guest} is the volume of the guest molecule obtained from its steric parameters (ref. 40 and Table S3). The MOF unit cell V_{MOF} of some of D-MIL-53⊃[DAT+guest] was estimated by PXRD peak positions using the program DICVOL[49] (Fig. S8, Table S3). For D-MIL-53⊃[DAT+guest] containing THF, $CHCl_3$, EtAc, *h*-Tol, EtOH, and AcNt as the guest, V_{MOF} was estimated by using the unit cell volume of MIL-53 (Fe)⊃guest[40], considering a linear relationship between the unit cell volumes of MIL-53 (Al)⊃guest and MIL-53 (Fe)⊃guest (Fig. S9).

References

1 Ladd, T. D. *et al.* Quantum computers. *Nature* **464**, 45-53, doi:10.1038/nature08812 (2010).

2 Arute, F. *et al.* Quantum supremacy using a programmable superconducting processor. *Nature* **574**, 505-510, doi:10.1038/s41586-019-1666-5 (2019).

3 Muralidharan, S. *et al.* Optimal architectures for long distance quantum communication. *Sci. Rep.* **6**, 20463, doi:10.1038/srep20463 (2016).

4 Bhaskar, M. K. *et al.* Experimental demonstration of memory-enhanced quantum communication. *Nature* **580**, 60-64, doi:10.1038/s41586-020-2103-5 (2020).

5 Degen, C. L., Reinhard, F. & Cappellaro, P. Quantum sensing. *Rev. Mod. Phys.* **89**, doi:10.1103/RevModPhys.89.035002 (2017).

6 Guo, X. *et al.* Distributed quantum sensing in a continuous-variable entangled network. *Nat. Phys.* **16**, 281-284, doi:10.1038/s41567-019-0743-x (2019).

7 Jing, M. *et al.* Atomic superheterodyne receiver based on microwave-dressed Rydberg spectroscopy. *Nat. Phys.* **16**, 911-915, doi:10.1038/s41567-020-0918-5 (2020).

8 Maze, J. R. *et al.* Nanoscale magnetic sensing with an individual electronic spin in diamond. *Nature* **455**, 644-647, doi:10.1038/nature07279 (2008).

9 Üngör, O., Ozvat, T. M., Ni, Z. & Zadrozny, J. M. Record Chemical-Shift Temperature Sensitivity in a Series of Trinuclear Cobalt Complexes. *J. Am. Chem. Soc.* **144**, 9132-9137, doi:10.1021/jacs.2c03115 (2022).

10 Zhang, T. *et al.* Toward Quantitative Bio-sensing with Nitrogen-Vacancy Center in Diamond. *ACS Sens.* **6**, 2077-2107, doi:10.1021/acssensors.1c00415 (2021).

11 Hendrickx, N. W. *et al.* A single-hole spin qubit. *Nat. Commun.* **11**, 3478, doi:10.1038/s41467-020-17211-7 (2020).

12 Gertler, J. M. *et al.* Protecting a bosonic qubit with autonomous quantum error correction. *Nature* **590**, 243-248, doi:10.1038/s41586-021-03257-0 (2021).

13 Jackson, C. E., Moseley, I. P., Martinez, R., Sung, S. & Zadrozny, J. M. A reaction-coordinate perspective of magnetic relaxation. *Chem. Soc. Rev.* **50**, 6684-6699, doi:10.1039/d1cs00001b (2021).

14 Wasielewski, M. R. *et al.* Exploiting chemistry and molecular systems for quantum information science. *Nat. Rev. Chem.* **4**, 490–504, doi:10.1038/s41570-020-0200-5 (2020).

15 Bader, K., Winkler, M. & van Slageren, J. Tuning of molecular qubits: very long coherence and spin-lattice relaxation times. *Chem. Commun.* **52**, 3623-3626, doi:10.1039/c6cc00300a (2016).

16 Giménez-Santamarina, S., Cardona-Serra, S., Clemente-Juan, J. M., Gaita-Arino, A. & Coronado, E. Exploiting clock transitions for the chemical design of resilient molecular spin qubits. *Chem. Sci.* **11**, 10718-10728, doi:10.1039/d0sc01187h (2020).

17 Yamashita, M. Next Generation Multifunctional Nano-Science of Advanced Metal Complexes with Quantum Effect and Nonlinearity. *Bull. Chem. Cos. Jpn.* **94**, 209-264, doi:10.1246/bcsj.20200257 (2021).

18 von Kugelgen, S. *et al.* Spectral Addressability in a Modular Two Qubit System. *J. Am. Chem. Soc.* **143**, 8069-8077, doi:10.1021/jacs.1c02417 (2021).

19 Jellen, M. J., Ayodele, M. J., Cantu, A., Forbes, M. D. E. & Garcia-Garibay, M. A. 2D Arrays of Organic Qubit Candidates Embedded into a Pillared-Paddlewheel Metal-Organic Framework. *J. Am. Chem. Soc.* **142**, 18513-18521, doi:10.1021/jacs.0c07251 (2020).

20 Yu, C. J., von Kugelgen, S., Laorenza, D. W. & Freedman, D. E. A Molecular Approach to Quantum Sensing. *ACS Cent. Sci.* **7**, 712-723, doi:10.1021/acscentsci.0c00737 (2021).

21 Zadrozny, J. M., Gallagher, A. T., Harris, T. D. & Freedman, D. E. A Porous Array of Clock Qubits. *J. Am. Chem. Soc.* **139**, 7089-7094, doi:10.1021/jacs.7b03123 (2017).

22 Harvey, S. M. & Wasielewski, M. R. Photogenerated Spin-Correlated Radical Pairs: From Photosynthetic Energy Transduction to Quantum Information Science. *J. Am. Chem. Soc.* **143**, 15508-15529, doi:10.1021/jacs.1c07706 (2021).

23 Bayliss, S. L. *et al.* Optically addressable molecular spins for quantum information processing. *Science* **370**, 1309–1312, doi:10.1126/science.abb9352 (2020).

24 Kirk, M. L., Shultz, D. A., Hewitt, P., Chen, J. & van der Est, A. Excited State Magneto-Structural Correlations Related to Photoinduced Electron Spin Polarization. *J. Am. Chem. Soc.* **144**, 12781-12788, doi:10.1021/jacs.2c03490 (2022).

25 Paquette, M. M., Plaul, D., Kurimoto, A., Patrick, B. O. & Frank, N. L. Opto-Spintronics: Photoisomerization-Induced Spin State Switching at 300 K in Photochrome Cobalt-Dioxolene Thin Films. *J. Am. Chem. Soc.* **140**, 14990-15000, doi:10.1021/jacs.8b09190 (2018).
26 McGuire, J., Miras, H. N., Donahue, J. P., Richards, E. & Sproules, S. Ligand Radicals as Modular Organic Electron Spin Qubits. *Chem. Eur. J.* **24**, 17598-17605, doi:10.1002/chem.201804165 (2018).
27 Christensen, J. A., Zhou, J., Tcyrulnikov, N. A., Krzyaniak, M. D. & Wasielewski, M. R. Spin-Polarized Molecular Triplet States as Qubits: Phosphorus Hyperfine Coupling in the Triplet State of Benzoisophosphinoline. *J. Phys. Chem. Lett.* **11**, 7569-7574, doi:10.1021/acs.jpclett.0c01912 (2020).
28 Mayländer, M., Chen, S., Lorenzo, E. R., Wasielewski, M. R. & Richert, S. Exploring Photogenerated Molecular Quartet States as Spin Qubits and Qudits. *J. Am. Chem. Soc.* **143**, 7050-7058, doi:10.1021/jacs.1c01620 (2021).
29 Kothe, G. *et al.* Initializing 2^{14} Pure 14-Qubit Entangled Nuclear Spin States in a Hyperpolarized Molecular Solid. *J. Phys. Chem. Lett.* **12**, 3647-3654, doi:10.1021/acs.jpclett.1c00726 (2021).
30 Jacobberger, R. M., Qiu, Y., Williams, M. L., Krzyaniak, M. D. & Wasielewski, M. R. Using Molecular Design to Enhance the Coherence Time of Quintet Multiexcitons Generated by Singlet Fission in Single Crystals. *J. Am. Chem. Soc.* **144**, 2276-2283, doi:10.1021/jacs.1c12414 (2022).
31 Kirner, S. V. *et al.* On-off switch of charge-separated states of pyridine-vinylene-linked porphyrin-C60 conjugates detected by EPR. *Chem. Sci.* **6**, 5994-6007, doi:10.1039/c5sc02051d (2015).
32 Kouno, H. *et al.* Nonpentacene Polarizing Agents with Improved Air Stability for Triplet Dynamic Nuclear Polarization at Room Temperature. *J. Phys. Chem. Lett.* **10**, 2208-2213, doi:10.1021/acs.jpclett.9b00480 (2019).
33 Sloop, D. J., Yu, H. L., Lin, T. S. & Weissman, S. I. Electron spin echoes of a photoexcited triplet: Pentacene in *p*-terphenyl crystals. *J. Chem. Phys.* **75**, 3746-3757, doi:10.1063/1.442520 (1981).
34 Yamauchi, S. Recent Developments in Studies of Electronic Excited States by Means of Electron Paramagnetic Resonance Spectroscopy. *Bull. Chem. Cos. Jpn.* **77**, 1255-1268, doi:10.1246/bcsj.77.1255 (2004).
35 Oxborrow, M., Breeze, J. D. & Alford, N. M. Room-temperature solid-state maser. *Nature* **488**, 353-356, doi:10.1038/nature11339 (2012).
36 Sun, L. *et al.* Room-Temperature Quantitative Quantum Sensing of Lithium Ions with a Radical-Embedded Metal–Organic Framework. *ChemRxiv*, doi:10.26434/chemrxiv-2022-rf8cp (2022).
37 Kultaeva, A., Pöppl, A. & Biktagirov, T. Atomic-Scale Quantum Sensing of Ensembles of Guest Molecules in a Metal-Organic Framework with Intrinsic Electron Spin Centers. *J. Phys. Chem. Lett.* **13**, 6737-6742, doi:10.1021/acs.jpclett.2c01429 (2022).
38 Férey, G. & Serre, C. Large breathing effects in three-dimensional porous hybrid matter: facts, analyses, rules and consequences. *Chem. Soc. Rev.* **38**, 1380-1399, doi:10.1039/b804302g (2009).
39 Loiseau, T. *et al.* A rationale for the large breathing of the porous aluminum terephthalate (MIL-53) upon hydration. *Chem. Eur. J.* **10**, 1373-1382, doi:10.1002/chem.200305413 (2004).
40 Millange, F., Serre, C., Guillou, N., Férey, G. & Walton, R. I. Structural effects of solvents on the breathing of metal-organic frameworks: an in situ diffraction study. *Angew. Chem. Int. Ed.* **47**, 4100-4105, doi:10.1002/anie.200705607 (2008).
41 Chandler, B. D. *et al.* Mechanical gas capture and release in a network solid via multiple single-crystalline transformations. *Nat. Mater.* **7**, 229-235, doi:10.1038/nmat2101 (2008).
42 Horike, S., Shimomura, S. & Kitagawa, S. Soft porous crystals. *Nat. Chem.* **1**, 695-704, doi:10.1038/nchem.444 (2009).
43 Schneemann, A. *et al.* Flexible metal-organic frameworks. *Chem. Soc. Rev.* **43**, 6062-6096, doi:10.1039/c4cs00101j (2014).
44 Fujiwara, S. *et al.* Triplet Dynamic Nuclear Polarization of Guest Molecules through Induced Fit in a Flexible Metal–Organic Framework. *Angew. Chem. Int. Ed.* **61**, e202115792, doi:10.1002/anie.202115792 (2022).
45 Stoll, S. & Schweiger, A. EasySpin, a comprehensive software package for spectral simulation and analysis in EPR. *J. Magn. Reson.* **178**, 42-55, doi:10.1016/j.jmr.2005.08.013 (2006).

46 Wrachtrup, J., Borczyskowski, C. v., Bernard, J., Orrit, M. & Brown, R. Optical detection of magnetic resonance in a single molecule. *Nature* **363**, 244–245, doi:10.1038/363244a0 (1993).
47 Fujiwara, S. *et al.* Triplet Dynamic Nuclear Polarization of Guest Molecules through Induced Fit in a Flexible Metal-Organic Framework. *Angew. Chem. Int. Ed.* **61**, e202115792, doi:10.1002/anie.202115792 (2022).
48 Yanai, N. *et al.* Gas detection by structural variations of fluorescent guest molecules in a flexible porous coordination polymer. *Nat. Mater.* **10**, 787-793, doi:10.1038/nmat3104 (2011).
49 Boultif, A. & Louër, D. Indexing of powder diffraction patterns for low-symmetry lattices by the successive dichotomy method. *J. Appi. Cryst.* **24**, 987-993, doi:10.1107/S0021889891006441 (1991).

Acknowledgments
This work was partly supported by the JST-FOREST Program (JPMJFR201Y), JSPS KAKENHI (JP20H02713, JP22K19051), JST SPRING (JPMJSP2136), the Innovation inspired by Nature Program of Sekisui Chemical Co. Ltd. Part of this work was conducted at Institute for Molecular Science, supported by Advanced Research Infrastructure for Materials and Nanotechnology (JPMXP1222MS0010), and by Nanotechnology Platform Program <Molecule and Material Synthesis> (JPMXP09S21MS0038), of the Ministry of Education, Culture, Sports, Science and Technology (MEXT), Japan. We would like to thank Dr. Ryo Ohtani and Mr. Yuuta Iwai for their help in structural analysis of MIL-53.

Author contributions
N. Y. conceived the project. A. Y. and N. Y. designed the experiments. A. Y. and S. F. prepared and characterized the samples, with the input of N. K. and N. Y. A. Y., M. A., T. F. and T, N. conducted the EPR measurements. A. Y. and N. Y. wrote the manuscript with contributions from all authors.

Competing interests
All authors declare that they have no competing interests.